TWO-LEVEL METHOD FOR 3D NON-RIGID REGISTRATION
With an Application to Statistical Atlases Construction

C. Wu*, P. E. Murtha**, A. B. Mor**, B. Jaramaz* **
* *Carnegie Mellon University, School of Computer Science*
Robotics Institute, Pittsburgh, PA, 15213
** *Institute for Computer Assisted Orthopaedic Surgery, The Western Pennsylvania Hospital Mellon Pavilion*
Suite 242, 4815 Liberty Avenue, Pittsburgh, PA 15224
chenyuwu@cmu.edu, PMurtha@icaos.org, abm@icaos.org, branko@icaos.org

Keywords: 3D deformable registration, Two-level method, Statistical atlas

Abstract: We propose a two-level method for 3D non-rigid registration and apply the method to the problem of building statistical atlases of 3D anatomical structures. 3D registration is an important problem in computer vision and a challenge topic in medical image field due to the geometrical complexity of anatomical shapes and size of medical image data. In this work we adopt a two-level strategy to deal with these problems. Compared with a general multi-resolution framework, we use an interpolation to propagate the matching instead of repeating registration scheme in each resolution. Our algorithm is divided into two main parts: a low-resolution solution to the correspondences and mapping of surface models using Chui and Rangarajan's robust point matching algorithm, followed by an interpolation to achieve high-resolution correspondences. Experimental results demonstrate our approach for solving the non-rigid registration and correspondences within complicated 3D data sets. In this paper we present an example of this method in the construction of a statistical atlas of the femur.

1 INTRODUCTION

Registration has been studied for years in computer vision, which is still a critical problem in medical image field due to the geometrical complexity of anatomical shapes, and computational complexity caused by the enormous size of volume data. It has numerous clinical applications such as statistical atlas construction for group study and statistical parameters analysis (Hill et al., 2001), mapping anatomical atlases to individual patient images for disease analysis (Fleute et al., 2002) and segmentation (Rohlfing et al., 2004).

According to the type of the transformation being applied, registration can be rigid or non-rigid. In other words, as long as the shape has no change between two images, the registration should be rigid, such as the intra-subject(same patient)-inter-modality(different imaging system) registration by capturing images at the same time. However, when we take into account the time, i.e., when two images are captured at different time, most of intra-subject registration will be non-rigid due to the shape variance of the anatomical structures for example swelling, prostate poking, bone fractures, tumor growth changes, intestinal movements etc. Besides, inter-subject(different patient) registrations are usually non-rigid because of the local anatomical differences between patients. Therefore, non-rigid (also known as deformable) registration has been an active topic in recent years. In general, a non-rigid transformation is represented by a global rigid or affine transformation plus a local non-linear deformation, which can be described by radial basis functions (RBF) (Yu, 2005), octree-spline (Szeliski and Lavallee, 1996), thin-plate spline (TPS) (Chui and Rangarajan, 2003), geometric splines (Farin, 1993), finite elements (Park et al., 1996), or free form B-spline (Rueckert et al., 2003) etc. In order to evaluate the registration, different similarity measurements have been utilized according to different features and imaging modalities. For example, sum of squared distances (SSD) is used for geometric features (Besl and McKay, 1992). For the intensity features, correlation coefficients (CC) (Kim and Fessler, 2004), Ratio Image Uniformity (RIU) (Woods et al., 1994), or mutual information (MI) (Wells et al., 1996) are usually considered. Registration problem can be simplified given some known correspondences, for example using markers (Maurer et al., 1997). Nevertheless, markers are not allowed to use or available in many scenarios. Alternate estimation of correspondences and transformations are therefore widely used for both rigid case (Besl and McKay, 1992) and non-rigid case (Chui and Rangarajan, 2003; Chui et al., 2004; Glaunes et al., 2004). Moreover, with the increase of data size and geometrical complexity, multi-resolution strategy has been adopted into the registration framework (Ellingsen and Prince, 2006; Jaume et al., 2002; Shen, 2002). Sparse ma-

trices are also used to handle the computational complexity (Papademetris et al., 2003).

In this paper we propose a two-level non-rigid registration approach for 3D surface mesh to deal with the computational and geometrical complexity, inspired by Chui and Rangarajan's non-rigid registration algorithm and the previous multi-resolution works. Since Chui and Rangarajan's algorithm is not able to handle more than 2000 3D points (Papademetris et al., 2003), in order to deal with more points, we break down the registration into a two-level process. We first apply their algorithm to the simplified low-resolution meshes (We use Garland's mesh simplification technique (Garland and Heckbert, 1997) to compute low-resolution meshes). And then, instead of successively matching in each resolution from coarse to fine, we directly propagate the correspondences from low resolution to the high resolution by an interpolation.

2 TWO-LEVEL REGISTRATION

2.1 Mesh Simplification

We use Garland's quadric error metrics (QEM) based mesh simplification (Garland and Heckbert, 1997) technique to obtain low-resolution meshes. QEM is based on the iterative contraction of vertex pairs. The cost of contraction is noted by a quadric error and the whole process is an iteratively minimizing the quadric error.

A critical parameter in the simplification is the number of vertices in the low-resolution meshes. The less vertices, the faster low-resolution registration but less accurate the high-resolution registration. We make a trade off between accuracy and speed by doing a series of experiments (See Sec. 4).

2.2 Low-Res Non-Rigid Registration

Point-to-Point Registration: We apply Chui and Rangarajan's non-rigid registration method on simplified meshes. Fuzzy correspondences and a deterministic annealing technique are adopted for a smoother optimization process and efficiency. A dual update strategy is utilized to estimate the correspondences and transformation iteratively. The non-rigid transformation is parameterized using thin-plate splines for a smooth spatial mapping.

Initial Alignment Before applying Chui and Rangarajan's method, we need an extra alignment due to the particularity of our data. Our data comes from CT scanned surfaces of human femur. Since we are more interested in condyles, As Fig. 1 shows, only distal femur is scanned to build meshes. According to different patients, some meshes include more femur shaft such as mesh Y, others include less shaft for example mesh X. Experiments shows that the registration might be very slow and may not converge for some cases, if we only move mesh X to the center of mesh Y at the very beginning. The reason is that some part of mesh Y (as showed in a blue rectangle) has no counterpart in mesh X, and we should not take into account this part in the registration. To tackle this problem, we estimate the pseudo center of mesh Y and a rigid transformation between two meshes.

As Fig. 1 illustrates, we use the height of mesh X to estimate the pseudo center of mesh Y. Assume axis z is the scan direction from the knee to hip, we estimate the pseudo center $\mathbf{c}_{Y'}$ as:

$$\mathbf{c}_{Y'} = \frac{1}{N_{Y'}} \sum_{(z_Y - \min z_Y) < (\max z_X - \min z_X)} \mathbf{p}_Y \qquad (1)$$

where $N_{Y'}$ covers points $\mathbf{p}_{Y'}$ in mesh Y that satisfy $(z_Y - \min z_Y) < (\max z_X - \min z_X)$ (black points in 1. We apply principal component analysis (PCA) to estimate the pose of each mesh. Assume

$$\mathbf{c}_X = \frac{1}{N_X} \sum \mathbf{p}_X \qquad (2)$$

is the center of mesh X. Then we can compute the covariance matrix for $\{\mathbf{p}_X\}$ and $\{\mathbf{p}_{Y'}\}$:

$$\begin{aligned} \Psi_X &= \tfrac{1}{N_X - 1} [\mathbf{p}_X^1 - \mathbf{c}_X, \cdots, \mathbf{p}_X^{N_X} - \mathbf{c}_X] \cdot [\mathbf{p}_X^1 - \mathbf{c}_X, \cdots, \mathbf{p}_X^{N_X} - \mathbf{c}_X]' \\ \Psi_{Y'} &= \tfrac{1}{N_X - 1} [\mathbf{p}_{Y'}^1 - \mathbf{c}_{Y'}, \cdots, \mathbf{p}_{Y'}^{N_{Y'}} - \mathbf{c}_{Y'}] \cdot [\mathbf{p}_{Y'}^1 - \mathbf{c}_{Y'}, \cdots, \mathbf{p}_{Y'}^{N_{Y'}} - \mathbf{c}_{Y'}]' \end{aligned} \qquad (3)$$

We compute the principle axes by decomposing the covariance matrix using moment analysis:

$$\Psi_X = \mathbf{U}_X \Lambda_X \mathbf{U}_X{}', \ \Psi_{Y'} = \mathbf{U}_{Y'} \Lambda_{Y'} \mathbf{U}_{Y'}{}' \qquad (4)$$

Each column of $\mathbf{U}_X$ represents an principle axis of points set $\{\mathbf{p}_X\}$, and $\mathbf{U}_{Y'}$ for $\{\mathbf{p}_{Y'}\}$. We use three axes to describe the pose of points set (Fig. 1): red for $\{\mathbf{p}_X\}$ and green for $\{\mathbf{p}_{Y'}\}$. We can estimate a rotation from axes of X to Y', which is given by $\mathbf{U}_{Y'} \cdot \mathbf{U}_X{}'$. Therefore, we can apply a rigid transformation $[\mathbf{U}_{Y'} \cdot \mathbf{U}_X{}' | (\mathbf{c}_{Y'} - \mathbf{c}_X)]$ to points set $\{\mathbf{p}_X\}$. Fig. 1 shows the transformed mesh X. Experiment shows the rate of convergence has been improved from 78% to 95.2%.

2.3 Local Non-Rigid Registration

Point-to-Surface Registration: In the previous section the non-rigid registration is applied to deform only points and SSD is used as a criteria. Here we will step further to minimize the SSD by using some points on the surface instead of original vertices. This idea is straightforward. As Fig. 2 shows, $\mathbf{x}_i$ is a point in the deformed mesh X, whose correspondence in mesh Y is $\mathbf{y}_i$. SSD ($\sum |\mathbf{x}_i - \mathbf{y}_i|^2$) has been minimized in the previous section. However, it is possible to decrease SSD

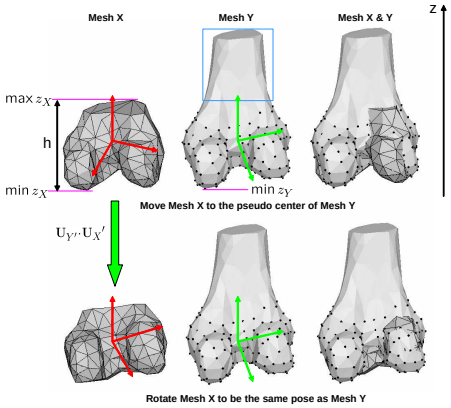

Figure 1: Illustration of the rigid transformation from mesh X to mesh Y. The first row compares the translated mesh X with Y. Black points in mesh Y are used to compute the pseudo center. The second compare the translated and rotated mesh X with Y. Red axes represent the principle components of point set in mesh X, blue axes for Y.

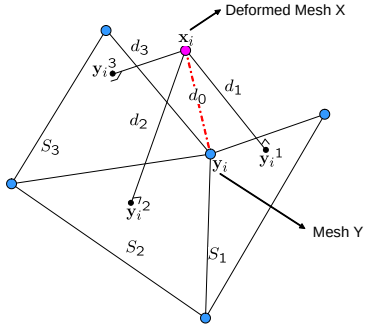

Figure 2: Illustration of local non-rigid registration between point and surface. $\mathbf{x}_i$ is a point in the deformed mesh X, whose correspondence in mesh Y is $\mathbf{y}_i$. The projection of $\mathbf{x}_i$ to each triangle S_t sharing $\mathbf{y}_i$ is denoted by $\mathbf{y}_i{}^t$. d_t is the distance between $\mathbf{x}_i$ and $\mathbf{y}_i{}^t$. $(t = 1,2,3,\cdots)$

more if we use some points on the surface instead of $\mathbf{y}_i$. Let's check the neighboring triangles of $\mathbf{y}_i$, which are triangles sharing the same vertex $\mathbf{y}_i$, for example S_1,S_2 and S_3 in Fig. 2. We examine the distance from $\mathbf{x}_i$ to each neighboring triangle, such as d_1, d_2 and d_3 in Fig. 2. If any of them is smaller than $d_0 = |\mathbf{x}_i - \mathbf{y}_i|$, we can use the corresponding projected point to replace $\mathbf{y}_i$ such that we can have achieve a smaller SSD.

Since the point-surface registration is a local process, we have to take into account the case that different points in mesh X which come up with the same corresponding surface point in mesh Y. We use a simple rule to handle such interference: the point in mesh X with smaller SSD will be updated with the surface point in mesh Y.

2.4 Low-Resolution to High-Resolution Interpolation

After the registration in low-resolution meshes, we directly apply a surface interpolation to those coarse meshes, in order to migrate the registration to high-resolution meshes. The problem is to build the correspondences between mesh X and Y, given correspondence between a subset of X and a subset of Y. Radial basis functions(RBF), finite element, multivariate spline such as thin-plate spline(2D bivariate spline) and triharmonic thin-plate spline, are popular techniques used in surface interpolation. Carr et al (Carr et al., 1997) include multivariate splines method into radial basis functions by using splines as kernel functions. In this work we use Gaussian kernel based RBF as an illustration due to it's simple mathematical representation and less restrictions on nodes. Specifically, we use a linear affine function plus a series of radial basis functions (RBFs) to construct the interpolation function:

$$\mathbf{y}_i^L = \underbrace{\mathbf{c_1} \cdot [\varphi(\|\mathbf{x}_i^L, \mathbf{x}_1^L\|), \cdots, \varphi(\|\mathbf{x}_i^L, \mathbf{x}_N^L\|)]' + \mathbf{c_2} + \mathbf{c_3} \cdot \mathbf{x}_i^L}_{g(\mathbf{x}_i^L)} \quad (5)$$

where $\mathbf{x}_i^L$ is a vertex in the low-resolution mesh X^L, whose correspondence in the low-resolution mesh Y^L is $\mathbf{y}_i^L$, $i = 1,2,\cdots,N$ (N is the number of vertices in mesh X^L). $\mathbf{x}_i^L$ and $\mathbf{y}_i^L$ are both 3×1 vectors with three coordinates. $\mathbf{c_1}$ is a $3\times N$ coefficient matrix of radial basis functions. $\varphi(\|\mathbf{x}_i^L, \mathbf{x}_j^L\|)$ are radially symmetric basis functions. We have chosen a Gaussian kernel $\varphi(\mathbf{u_i}, \mathbf{u_j}) = \exp(-\|\mathbf{u_i} - \mathbf{u_j}\|/0.5)$, as suggested by (Pighin et al., 1998). $\mathbf{c_2}$ and $\mathbf{c_3}$ are coefficients for the affine component. $\mathbf{c_2}$ is a 3×1 vector and $\mathbf{c_3}$ is a 3×3 matrix. Given N correspondences, we have N equations for each axis ($\mathcal{X}$, $\mathcal{Y}$ and $\mathcal{Z}$):

$$\underbrace{\begin{bmatrix} \varphi(\mathbf{x}_1^L, \mathbf{x}_1^L) \cdots \varphi(\mathbf{x}_1^L, \mathbf{x}_N^L) & 1 & \mathbf{x}_1^{L\,T} \\ \vdots & & \\ \varphi(\mathbf{x}_N^L, \mathbf{x}_1^L) \cdots \varphi(\mathbf{x}_N^L, \mathbf{x}_N^L) & 1 & \mathbf{x}_N^{L\,T} \end{bmatrix}}_{\mathbf{P}^k} \cdot \underbrace{\begin{bmatrix} \mathbf{c_1^k{}^T} \\ \mathbf{c_2^k{}^T} \\ \mathbf{c_3^k{}^T} \end{bmatrix}}_{\mathbf{c}^k} = \underbrace{\begin{bmatrix} \mathbf{y}_1^{L\,k} \\ \vdots \\ \mathbf{y}_N^{L\,k} \end{bmatrix}}_{\mathbf{y}^{L\,k}} \quad (6)$$

where $\mathbf{c_1}^k$, $\mathbf{c_2}^k$ and $\mathbf{c_3}^k$ denote the k^{th} row of $\mathbf{c_1}$, $\mathbf{c_2}$ and $\mathbf{c_3}$, respectively. $\mathbf{y}_i^{L\,k}$ denotes the k^{th} row of $\mathbf{y}_i^L$, k can be 1,2 or 3, corresponding to the $\mathcal{X}$, $\mathcal{Y}$, and $\mathcal{Z}$ axes. Therefore we have $3N$ equations in all:

$$\mathbf{P} = [\mathbf{P}^1, \mathbf{P}^2, \mathbf{P}^3]', \mathbf{c} = [\mathbf{c}^1, \mathbf{c}^2, \mathbf{c}^3]', \mathbf{y} = [\mathbf{y}^1, \mathbf{y}^2, \mathbf{y}^3]' \quad (7)$$

$\mathbf{P}$ is a $3N\times(N+4)$ matrix. In order to ensure a smooth interpolation function, we add the additional orthogonality constraints $\sum_i \mathbf{x}_i^{L\,T} \mathbf{c_{1,i}} = 0$ (Carr et al., 2001) to Eq. 6, where $\mathbf{c_{1,i}}$ denotes the i^{th} column of $\mathbf{c_1}$:

$$\underbrace{\begin{bmatrix} & \mathbf{P} & & & \\ \mathbf{x}_1^L & \mathbf{x}_2^L & \cdots & \mathbf{x}_N^L & \mathbf{0}_{4\times 4} \end{bmatrix}}_{\mathbf{Q}} \cdot \mathbf{c} = \underbrace{\begin{bmatrix} \mathbf{y} \\ \mathbf{0}_{4\times 1} \end{bmatrix}}_{\mathbf{w}} \quad (8)$$

The least-squares solution for this linear system, $\mathbf{Qc} = \mathbf{w}$, is given by $\mathbf{c} = (\mathbf{Q}^T\mathbf{Q})^{-1}\mathbf{Q}^T\mathbf{w}$.

Finally, the correspondence of a vertex $\mathbf{x}_j^H$ in the high-resolution mesh X^H can be computed by using Eq. 5: $\mathbf{y}_j^H = g(\mathbf{x}_j^H)$, for $j = 1,\cdots,M$ (M is the number of vertices in mesh X^H). We also apply the local non-rigid registration for $\mathbf{y}_j^H$ as described in Sec. 2.3.

3 APPLICATION: FEMUR ATLAS CONSTRUCTION

Statistical anatomical atlases are one of powerful analysis tool for 2D and 3D medical images (Cootes et al., 1995; Cootes and Taylor, 2001). Due to the anatomical variance between subjects, construction of statistical anatomical atlases usually requires non-rigid registrations between individual models. As an application, we apply our registration results to build a statistical atlas for an anatomical structure. A rigid pose alignment has been applied to eliminate the effect of imaging pose (Goryn and Hein, 1995) before atlas construction.

Suppose we have K aligned meshes and each mesh can be represented by a $3M\times 1$ vector $\mathbf{v}_i (i=1,\cdots,K)$, where M is the number of points in each mesh and 3 denotes three coordinates $\mathcal{X}$, $\mathcal{Y}$, and $\mathcal{Z}$. We compute the mean vector $\mathbf{c}=\frac{1}{K}\sum \mathbf{v}$ and covariance matrix $\Psi = \frac{1}{M-1}[\mathbf{v}^1-\mathbf{c},\cdots,\mathbf{v}^K-\mathbf{c}]\cdot[\mathbf{v}^1-\mathbf{c},\cdots,\mathbf{v}^K-\mathbf{c}]'$ and then apply PCA: $\Psi = \mathbf{U}\Lambda\mathbf{U}'$.

Therefore, any mesh vector in the data set can be represented by a mean vector plus a linear combination of each principal components (each column of U):

$$\mathbf{v}_i = \mathbf{c} + \mathbf{U}\eta_i \tag{9}$$

where η_i is a $K\times 1$ coefficient vector obtained by project $\mathbf{v}_i$ onto each principal axis. New models, not included in the data set, can be generated by manipulating the elements of η_i.

4 EXPERIMENTAL RESULTS

87 CT-scanned 87 patients with healthy femur: 53 males and 34 females; 43 left femurs and 44 right. The patients age from 39 to 78 and their femur height ranges from 400mm to 540mm. The CT volumes are segmented to provide triangulated surface models using Marching Cube algorithm. All surface models are smoothed by the method in (Desbrun et al., 1999). Each femur data includes two mesh surfaces: femoral head and distal femur.

Fig. 3 shows two high-resolution mesh X^H (21130 vertices, 42256 triangles, 65.84mm in z-axis) and Y^H (26652 vertices, 53300 triangles, 105.89mm in z-axis) for distal femur (Patient X is a 79 years old female, with 472.55mm height femur; Patient Y is a 53 years old female, with 477.59mm height femur). We compute point-to-surface distance from X^H to Y^H (Aspert et al., 2002):

$$d(p,Y^H) = \min_{p'\in Y^H} \|p-p'\|_2, p\in X^H \tag{10}$$

where $\|\cdot\|_2$ is Euclidean norm. The HSV color of each vertex in mesh X^H denotes the distance $d(p,Y^H)$. We also compute the mean error $d_m(X^H,Y^H)$ and root mean square error $d_{RMS}(X^H,Y^H)$ between mesh X^H and Y^H.

$$\begin{aligned} d_m(X^H,Y^H) &= \tfrac{1}{|X^H|}\int\int_{p\in X^H} d(p,Y^H)dX^H \\ d_{RMS}(X^H,Y^H) &= \sqrt{\tfrac{1}{|X^H|}\int\int_{p\in X^H} d(p,Y^H)^2 dX^H} \end{aligned} \tag{11}$$

With respect to the bounding box diagonal of mesh Y^H(158.48mm), the mean error is 6.49% and root mean square error is 7.70%. Fig. 4 shows the low-resolution mesh X^L (169 vertices, 334 triangles) and Y^L (213 vertices, 422 triangles) after simplification. With respect to the bounding box diagonal of mesh Y^L(158.28mm), the mean error is 6.53% and root mean square error is 7.74%. Fig. 5 shows the deformed low-resolution mesh $X^{L(1)}$ and Y^L after applying Chui and Rangarajan's non-rigid registration. With respect to the bounding box diagonal of mesh Y^L(158.28mm), the mean error is 1.68% and root mean square error is 2.13%. Surface distance has been significantly decreased after Chui and Rangarajan's non-rigid registration. Fig. 6 shows the deformed low-resolution mesh $X^{L(2)}$ and Y^L after applying a local deformation discussed in Sec. 2.3. With respect to the bounding box diagonal of mesh Y^L(158.28mm), the mean error is 0.68% and root mean square error is 1.42%, which shows local point-to-surface registration can decrease the surface distance further. Fig. 7 shows the interpolated high-resolution mesh $X^{H(1)}$ and Y^H after applying an interpolation. With respect to the bounding box diagonal of mesh Y^H(158.48mm), the mean error is 1.65% and root mean square error is 2.10%. The reason why the surface distance slightly increases after interpolation is: only 0.80% of vertices in mesh $X^{H(1)}$ have correspondences obtained by non-rigid registration, others obtain correspondences by interpolation. Fig. 8 shows the deformed high-resolution mesh $X^{H(2)}$ and Y^H after applying a local deformation discussed in Sec. 2.3. With respect to the bounding box diagonal of mesh Y^H(158.48mm), the mean error is 0.28% and root mean square error is 1.26%, which once again demonstrates that local point-to-surface registration is helpful for decreasing the surface distance.

The critical parameter in our algorithm is the number of vertices N used in the low-resolution meshes, which affects the computational complexity and accuracy. Due to the different length of femur shaft within different meshes, we choose a mesh as a reference such that we could compare any other mesh with this reference, following the procedure showed in Fig. 3-8. By tuning the number N_{ref}, we can make a trade off between accuracy and efficiency (in order to maintain the same points density, we set $N_{other} = N_{ref}\times height_{other}/height_{ref}$).

Moreover, in the application of atlas construction, we can choose N_{ref} by comparing the reconstructed

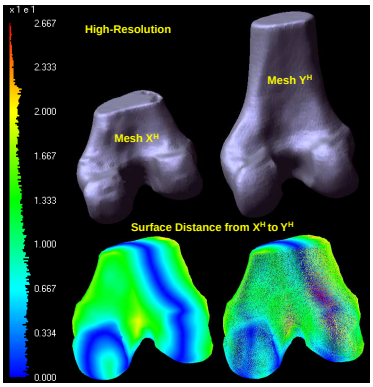

Figure 3: Input high-resolution meshes.

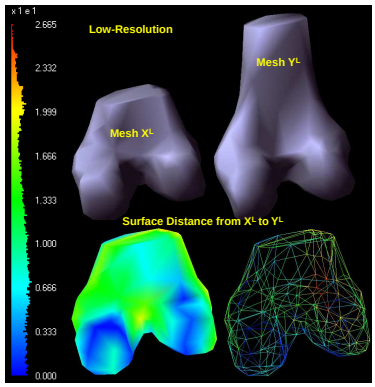

Figure 4: After simplification.

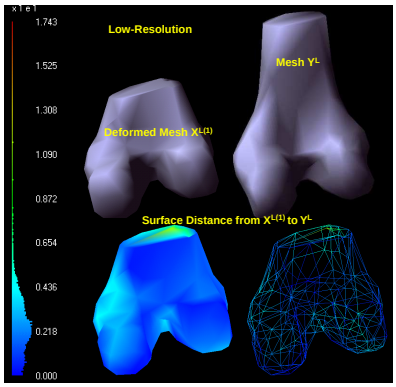

Figure 5: After low-resolution registration.

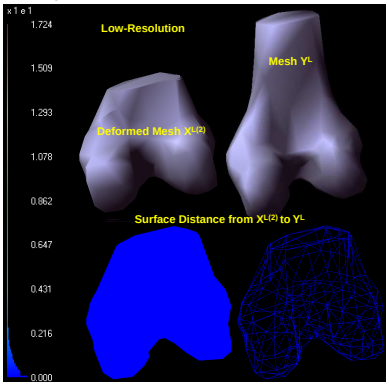

Figure 6: After local deformation.

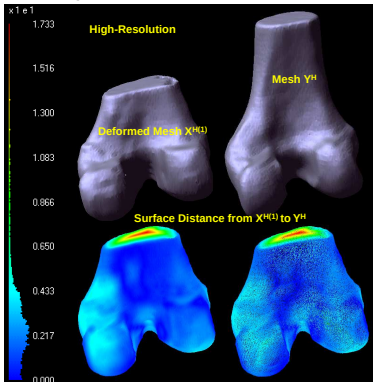

Figure 7: After interpolation.

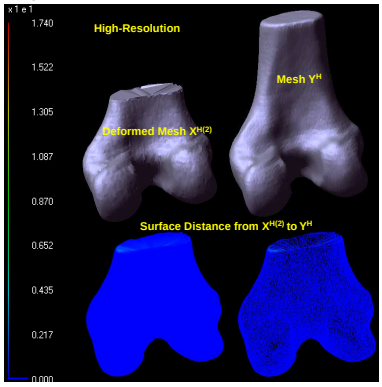

Figure 8: After local deformation.

mesh from atlas with the original mesh, such that we can also ensure the generality and accuracy of the atlas. We conduct a series of leave-one-out experiments. We first select a reference mesh(which has all correspondences in any other meshes in the data set) and then change N_{ref}. For each N^t_{ref}, we compute $N^t_{other}(other = 1,\cdots,K, other \neq ref)$ for other meshes and apply the two-level non-rigid registration. After that, with K aligned meshes we apply K leave-one-out experiments: for any $\mathbf{v}_i(i = 1,\cdots,K)$, we use other $K-1$ to construct an atlas using PCA (Sec. 3). Let $\mathbf{U}^S_i$ denote the first S columns of the principal component matrix $\mathbf{U}_i$, which consists of 95% energy. Then $\mathbf{v}_i(i = 1,\cdots,K)$ can be reconstructed by this atlas:

$$\widetilde{\mathbf{v}}_i = \mathbf{c} + \mathbf{U}^S_i \mathbf{U}^{S^T}_i (\mathbf{v}_i - \mathbf{c}) \qquad (12)$$

We compare the surface distance between each pair of mesh V_i and $\widetilde{V}_i$ and obtain the average mean error and root mean square error for each N^t_{ref}:

$$\overline{d^t_m} = \frac{1}{K} d_m(V_i, \widetilde{V}_i),\ \overline{d^t_{RMS}} = \frac{1}{K} d_{RMS}(V_i, \widetilde{V}_i) \qquad (13)$$

By changing N^t_{ref} we can compute different $\overline{d^t_m}$ and $\overline{d^t_m}$, also processing time $\overline{T^t}$ of two-level registration. Fig. 9 shows when $N^t_{ref} \geq 290$, $\overline{d^t_m}$ will be less than 1mm, which is a practical number in clinical application. Fig. 10 shows when $N^t_{ref} \geq 330$, average processing time of registration of two meshes will exceed 5 mins (2.4GHz Pentium PC with 1G RAM). Compared with original Chui and Rangranjan's algorithm, ours only need 5 mins for registering any size of meshes (interpolation costs less than 1sec when the number of vertices is less than 200,000), however, their method costs 5 mins for 350 vertices, 10 mins for 460 vertices, 20 mins for 610 vertices, etc. Our algorithm significantly improve the efficiency without losing accuracy.

Finally we select $N^t_{ref} = 290$ and construct atlases for distal femur, femoral head, and entire femur, respectively. Fig. 11 shows the energy in terms of principal components in each atlas.

5 CONCLUSION

In this paper we have developed a two-level algorithm to tackle the registration problem due to the geometrical and computational complexity. Experiments demonstrate our algorithm significantly improve the efficiency without decreasing accuracy, by comparing with the original Chui and Rangranjan's algorithm. Some interesting issues such as gender effect for the atlases, interpolation with other kernel functions, etc will be addressed in the future work.

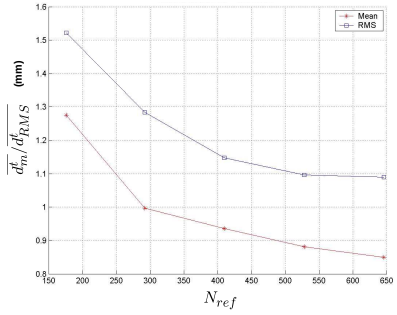

Figure 9: Reconstruction error $\overline{d_m}$ and $\overline{d_{RMS}}$ in terms of N_{ref}.

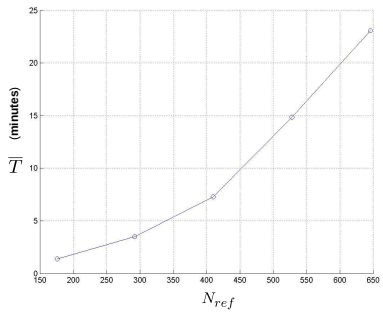

Figure 10: Registration processing time $\overline{T}$ in terms of N_{ref}.

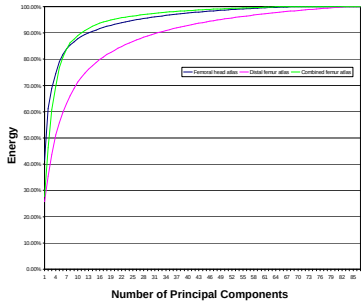

Figure 11: Atlases of distal femur(pink), femoral head(blue) and entire femur(green).

REFERENCES

Aspert, N., Santa-Cruz, D., and Ebrahimi, T. (2002). Mesh: measuring errors between surfaces using the hausdorff distance. In *Proc. ICME'02*, volume 1, pages 705–708.

Besl, P. and McKay, N. (1992). A method for registration of 3-d shapes. In *IEEE Trans. on PAMI'92*, volume 14, pages 239–256.

Carr, J. C., Beatson, R. K., Cherrie, J. B., Mitchell, T. J., Fright, W. R., Mccallum, B. C., and Evans, T. R. (2001). Reconstruction and representation of 3d objects with radial basis functions. In *Proc. SIGGRAPH'01*, pages 67–76.

Carr, J. C., Fright, W. R., and Beatson, R. K. (1997). Surface interpolation with radial basis functions for medical imaging. In *IEEE Trans. on Medical Imaging*, volume 16, pages 96–107.

Chui, H. and Rangarajan, A. (2003). A new point matching algorithm for non-rigid registration. In *Computer Vision and Image Understanding*, volume 89, pages 114–141.

Chui, H., Rangarajan, A., Zhang, J., and Leonard, C. M. (2004). Unsupervised learning of an atlas from unlabeled point-sets. In *IEEE Trans. on PAMI'04*, volume 2, pages 160–172.

Cootes, T. and Taylor, C. (2001). Statistical models of appearance for medical image analysis and computer vision. In *Proc. SPIE Image Processing*, volume 4322, pages 238–248.

Cootes, T., Taylor, C., Cooper, D., and Graham, J. (1995). Active shape models: their training and application. In *Computer Vision and Image Understanding*, volume 61, pages 38–59.

Desbrun, M., Meyer, M., Schroder, P., and Barr, A. (1999). Implicit fairing of irregular meshes using diffusion and curvature flow. In *Proc. SIGGRAPH'99*, pages 317–324.

Ellingsen, L. M. and Prince, J. L. (2006). Deformable registration of ct pelvis images using mjolnir. In *Proc. SPIE Medical Imaging Conference*, volume 6144, pages 329–337.

Farin, G. (1993). Curves and surfaces for cagd. In *Academic Press*. New York.

Fleute, M., Lavallée, S., and Desbat, L. (2002). Integrated approach for matching statistical shape models with intra-operative 2d and 3d data. In *Proc. MICCAI'02*, volume 2, pages 364–372.

Garland, M. and Heckbert, P. (1997). Surface simplification using quadric error metrics. In *Proc. SIGGRAPH'97*, pages 209–216.

Glaunes, J., Trouvé, A., and Younes, L. (2004). Diffeomorphic matching of distributions: a new approach for unlabelled point-sets and sub-manifolds matching. In *Proc. CVPR'04*, volume 2, pages 712–718.

Goryn, D. and Hein, S. (1995). On the estimation of rigid body rotation from noisy data. In *IEEE Trans. on PAMI'95*, volume 17, pages 1219–1220.

Hill, D., Batchelor, P., Holden, M., and Hawkes, D. (2001). Medical image registration. In *Physics in Medicine and Biology*, volume 46, pages 1–45.

Jaume, S., Macq, B., and Warfield, S. K. (2002). Labeling the brain surface using a deformable multiresolution mesh. In *Proc. MICCAI'02*, pages 451–458.

Kim, J. and Fessler, J. A. (2004). Intensity-based image registration using robust correlation coefficients. In *IEEE Trans. on PAMI'04*, volume 23, pages 1430–1444.

Maurer, C. R., Fitzpatrick, J. M., Wang, M. Y., Galloway, R. L., Maciunas, R. J., and Allen, G. G. (1997). Registration of head volume images using implatable fiducial markers. In *IEEE Trans. on PAMI'97*, volume 16, pages 447–462.

Papademetris, X., Jackowski, A., Schultz, R., Staib, L., and Duncan, J. (2003). Non-rigid brain registration using extended robust point matching for composite multisubject fmri analysis. In *Proc. MICCAI'03*, volume 2879, pages 788–795.

Park, J., Mataxas, D., Young, A., and Axel, L. (1996). Deformable models with parameter functions for cardiac motion analysis from tagged mri data. In *IEEE Trans. on Medical Imaging*, volume 15, pages 278–289.

Pighin, F., Hecker, J., Lischnski, D., Szeliski, R., and Salesin, D. (1998). Synthesizing realistic facial expressions from photographs. In *Proc. SIGGRAPH'98*, pages 75–84.

Rohlfing, T., Russakoff, D., and Maurer, C. (2004). Performance-based classifier combination in atlas-based image segmentation using expectation-maximization parameter estimation. In *IEEE Trans. on Medical Imaging*, volume 23, pages 983–994.

Rueckert, D., Frangi, A., and Schnabel, J. (2003). Automatic construction of 3-d statistical deformation models of the brain using nonrigid registration. In *IEEE Trans. on Medical Imaging*, volume 22, pages 1014–1025.

Shen, D. Davatzikos, C. (2002). Hammer: hierarchical attribute matching mechanism for elastic registration. In *IEEE Trans. on Medical Imaging*, volume 21, pages 1421–1439.

Szeliski, R. and Lavallee, S. (1996). Matching 3-d anatomical surfaces with non-rigid deformations using octree-splines. In *IJCV'96*, volume 18, pages 171–186.

Wells, W. M., Viola, P., Atsumi, H., Nakajima, S., and Kikinis, R. (1996). Multi-modal volume registration by maximization of mutual information. In *Medical Image Analysis*, volume 1, pages 35–51.

Woods, R. P., Mazziotta, J. C., and Cherry, S. R. (1994). Mri-pet registration with automated algorithm. In *Journal of Computer Assisted Tomography*, volume 17, pages 536–546.

Yu, H. (2005). Automatic rigid and deformable medical image registration. In *Ph.D. Dissertation, Mechanical Engineering Department, Worcester Polytechnic Institute, Worcester, MA*.